Geoscience Letters

RESEARCH LETTER

Open Access

The 2022 M_w6.2 Pasaman, Indonesia, earthquake sequence and its implication of seismic hazard in central-west Sumatra

Rizki Wulandari[1,4], Chung-Han Chan[1,2,4*] and Adhi Wibowo[3]

Abstract

The 2022 M_w6.2 Pasaman earthquake took place in central-west Sumatra in association with activity in the Sumatran Fault system. This study clarifies the spatial and temporal distribution of the Pasaman earthquake sequence and forecasts the earthquake sequence's impact on the seismicity in the vicinity and in the Sumatran Fault system. We first examined the seismicity before the mainshock and observed temporal low *b*-value anomalies, shedding light on the earthquake's precursor by monitoring *b*-values prior to the event. Based on the aftershocks in the first 18 days, we modeled the temporal distribution of the aftershocks according to the modified Omori's law, which suggested this sequence could last 49–473 days. By further considering Båth's law and the Gutenberg–Richter law, we estimated the temporal distribution of the maximum magnitudes in the aftershock sequence. To understand the spatial pattern of the aftershocks, we calculated the coseismic Coulomb stress change imparted by the Pasaman mainshock. Considering uncertainties of the Coulomb stress calculations from rupture geometry, mainshock parameters, friction coefficients, and strike angles of the receiver plane, the patterns of the Coulomb stress changes are similar that the stress increases extended northwest and southeast, consistent with aftershock distribution. We further evaluated rupture probability for each segment of the Sumatran Fault. Considering the stress perturbation imparted by the Pasaman earthquake, we expected a seismicity rate increase of ca. 40% at the Sumpur and Sianok segments in the short term. To quantify long-term rupture probability, the recurrence interval and the time elapsed since the previous earthquake were incorporated based on the time-dependent Brownian passage-time model. The earthquake probability at the Sumani segment in the coming 50 years was determined to be 72%. The results of this study have significant implications for subsequent probabilistic seismic hazard assessments, not only for Sumatra but also for certain metropolitan areas in Malaysia and Singapore.

Keywords Pasaman earthquake, Aftershock, *b*-value, Coulomb stress changes, Omori's law, Earthquake forecasting, Sumatran fault, And Sumatra

*Correspondence:
Chung-Han Chan
hantijun@googlemail.com
Full list of author information is available at the end of the article

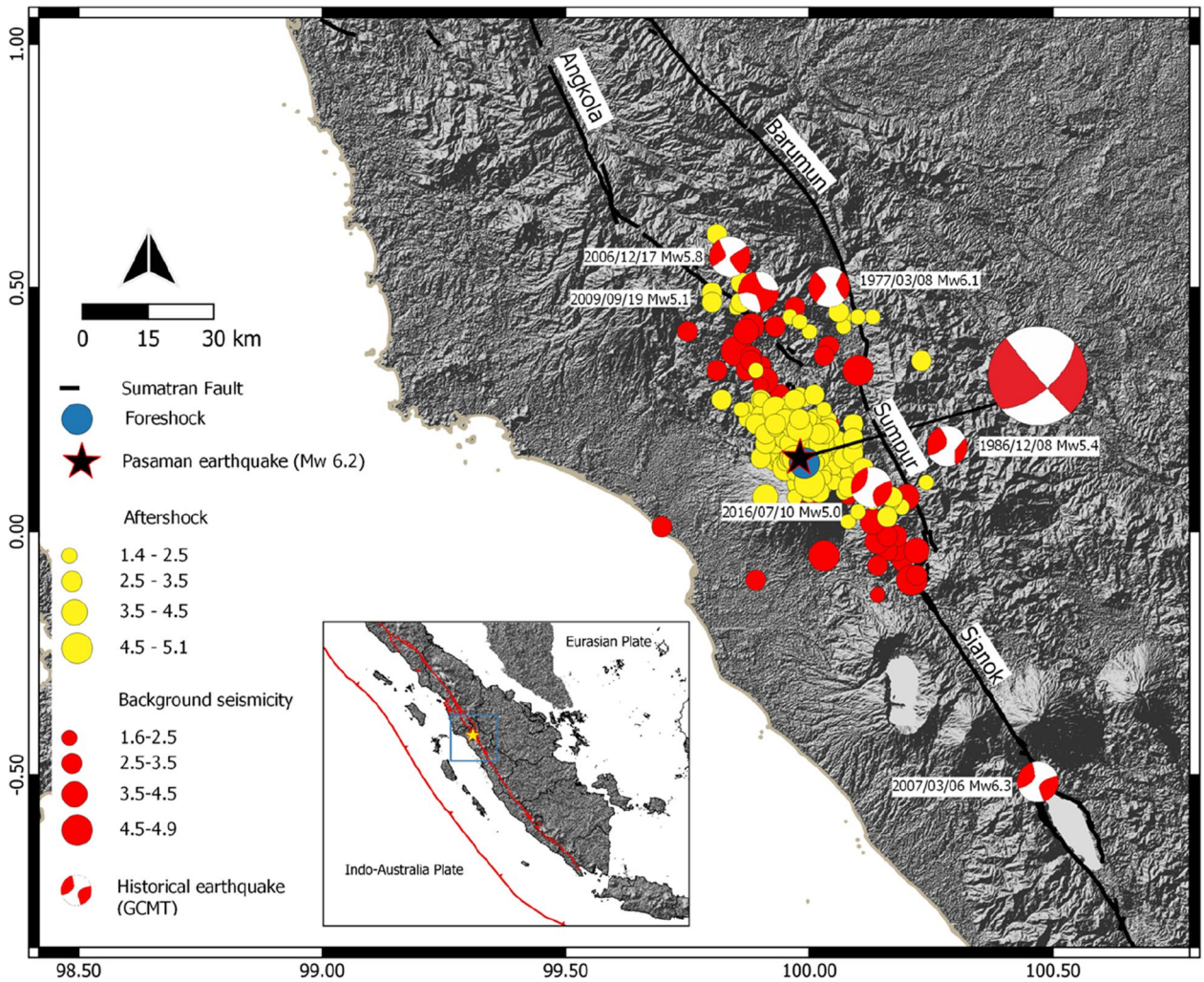

Fig. 1 Distribution of seismicity before (red circles) and after (yellow circles) the Pasaman earthquake (star). The foreshock with M_w5.2 is shown by a blue circle. The focal mechanism of the Pasaman and earthquake and previous events were determined by BMKG and USGS, respectively. The black lines denote fault alignments of the Sumatran Fault (Sieh & Natawidjaja 2000)

Introduction

An M_w6.2 earthquake known as the Pasaman earthquake occurred on February 25, 2022, in Pasaman, Indonesia (Fig. 1). This event was a shallow earthquake with a hypocentral depth of 12.6 km, determined by the Agency of Meteorology, Climatology, and Geophysics (also known as 'BMKG') or 4.0 km, determined by the U.S. Geological survey (also known as 'USGS'). Based on the focal mechanisms determined by BMKG, this earthquake was a result of strike-slip faulting (Table 1), which could be associated with activity in the Sumatran Fault system near the Angkola, Barumun, Sumpur, and Sianok segments, as shown in Fig. 1 (Sieh and Natawidjaja 2000). In this earthquake sequence, one foreshock with M_w5.2 occurred four minutes before the mainshock, and 217 aftershocks were recorded within 18 days (Fig. 1). This sequence took place in the Sumatran Fault system and filled the fault alignment gap between the Angkola and Sianok segments. The occurrence of this sequence makes it urgent to clarify whether the seismicity activity in the fault system will be activated.

Based on the intensity map proposed by BMKG (https://twitter.com/infoBMKG/status/1497028636012351488), the Pasaman earthquake not only resulted in strong ground motion in the vicinity of the earthquake with a Modified Mercalli Intensity (MMI) value of V, but was also felt as far away as Malaysia and Singapore with a value of II on the MMI scale. The ground shaking in the far field could be attributed to ground motion attenuation behavior (Megawati et al. 2003) and soft soil

Table 1 The source parameters of the Pasaman earthquake determined by the Agency of Meteorology, Climatology, and Geophysics (BMKG)

Date	Latitude (°N)	Longitude (°E)	Depth (km)	M_w	Strike (°)	Dip (°)	Rake (°)	Length (km)[a]	Width (km)[a]	Right lateral slip (m)	Dip slip (m)
2/25/2022	0.15	99.98	12.6	6.2	133	76	175	17.99	8.45	0.484	0.042
					224	85	13				

[a] The length and the width were estimated based on the empirical relations of Wells and Coppersmith (1994)

amplification (Walling et al. 2012). Based on the characteristics of the path and site effects, the next large event could result in significantly larger ground shaking for the surrounding region, even in the metropolises of Malaysia and Singapore. Thus, it is crucial to understand the behavior of the seismicity activity and assess potential seismic hazard in this region.

Various models have been proposed to illustrate spatial and temporal patterns of seismicity. Seismic activity could be presented by a frequency–magnitude distribution and modeled by the Gutenberg–Richter relation (also known as the GR law, Gutenberg and Richter 1944), expressed as:

$$\log_{10} N = a - bM, \tag{1}$$

where N represents the cumulative number of earthquakes with magnitudes larger than M, and a and b are constants obtained through regression. Previous studies (e.g., Schorlemmer et al. 2005) indicated that the b-value was related to the stress conditions, that is, a low b-value in a region implies a large differential stress, inferring that this region is toward the end of a seismic cycle. Thus, a b-value anomaly could be regarded as an indicator of forthcoming large earthquakes (e.g., Chan et al. 2012a).

After a significant earthquake, one of the major concerns is duration of aftershocks. To quantify the aftershock rate evolution, the modified Omori's law (Utsu 1961) modeled the seismicity rate as a function of the time elapsed after a mainshock, expressed as:

$$n(t) = \frac{K}{(C+t)^P}, \tag{2}$$

where $n(t)$ represents the seismicity rate as a function of time t since the mainshock, K represents the amplitude of the rate, C represents the time delay of rate decay, and P represents the decay rate. By comparing with the background seismicity rate, the aftershock duration could be estimated. Considering the end time (t_{end}) of the aftershock duration, the number of remaining aftershocks (N_1) since time t_1 could be evaluated (Chan and Wu 2013), represented as follows:

$$N_1 = \int_{t_1}^{t_{\text{end}}} \frac{K}{(C+t)^P} \mathrm{dt}. \tag{3}$$

Understanding the temporal evolution of maximum magnitude also needs to be a concern for understanding aftershock behavior. Båth (1965) states the average magnitude difference (ΔM) of its maximum largest aftershock (M_1) with the mainshock (M_0) to be about 1.2. Additionally, previous studies (e.g., Chan and Wu 2013) suggested that ΔM could be regarded as a variable that is larger than the expected value of $1/\beta$, as follows:

$$\beta = b \cdot \ln(10), \tag{4}$$

where b is the b-value modeled by the GR law of aftershock events.

In addition, considering the ratio of N_1 (Eq. 3) to $n(t)$ (Eq. 2) for various times, the decay of the maximum aftershock can be modeled (Chan and Wu 2013).

Rupture on a fault plane causes deformation in the vicinity, which can be converted into Coulomb stress change (ΔCFS). Previous studies (e.g., King et al. 1994) concluded that an increase in Coulomb stress could trigger aftershocks or even a subsequent larger earthquake. Coulomb stress change has become a crucial type of analysis particularly for the assessment of large earthquakes in the future (Wang et al. 2014). For example, the 2005 M_w8.7 Nias earthquake is one of the successful case studies of stress triggering by the 2004 M_w9.2 Sumatra–Andaman in Indonesia (Hughes et al. 2010). The ΔCFS can be expressed as (Harris and Simpson 1998):

$$\Delta\text{CFS} = \Delta\tau + \mu_s' \Delta\sigma_e, \tag{5}$$

Where $\Delta\tau$ is shear stress, $\Delta\sigma_e$ is the normal stress, and μ_s' is the effective friction coefficient, usually between 0.2 and 0.8. ΔCFS calculation could be solved in a region and on a specific fault plane (Chan et al. 2017).

A ΔCFS model could not only illustrate the spatial distribution of subsequent earthquakes but also be further converted to time-dependent seismicity rate evolution,ΔR(t), by the rate-and-state friction model (Dieterich 1994) and further modified by Chan et al. (2017), expressed as:

$$\Delta R(t) = \frac{\lambda}{\left[\exp\left(-\frac{\Delta CFS}{A\sigma}\right) - 1\right]\exp\left(-\frac{t-t_n}{t_{\text{na}}}\right) + 1}, \tag{6}$$

where λ represents the long-term seismicity rate; $A\sigma$ represents a constitutive parameter of the model; t_n represents the occurrence time of the earthquake that caused the ΔCFS; and t_{na} represents the aftershock duration.

Based on the models mentioned above, this study aims to clarify the seismicity activity of the Pasaman earthquake sequence and to forecast the seismicity in this region and the Sumatran Fault system. We first analyzed seismicity activity before the Pasaman mainshock to clarify the possible precursory index based on the temporal evolution of the b-value. We then forecast the aftershock behaviors based on the modified Omori's law, Båth's law, and the coseismic Coulomb stress change. In addition,

we evaluated the rupture probability for each segment of the Sumatran Fault considering the impact of the Pasaman earthquake and parameters of each fault segment.

Seismicity activity and *b*-value anomaly before the Pasaman earthquake.

To investigate the seismicity in the study region, we accessed the earthquake catalog summarized by BMKG. To satisfy our hypothesis, dependent events (foreshocks and aftershocks) have been removed from the earthquake catalog using the declustering algorithm by Gardner and Knopoff (1974).

On the distribution of background seismicity (Fig. 1), most of the seismicity before the Pasaman earthquake sequence was located on the Angkola and Sianok segments of the Sumatran Fault, where a few background events happened near the Pasaman earthquake mainshock. To understand the evolution of seismic activity in the study region, we modeled the pattern of the frequency–magnitude distribution using the GR law. In this study, the GR law regression was based on a maximum-likelihood estimation (Aki 1965; Utsu 1965).

To clarify whether there was a *b*-value anomaly before the Pasaman earthquake, we estimated a temporal variation in *b*-values for the seismicity within a radius of 40 km of the epicenter according to the ZMAP software (Wiemer et al. 2001). To obtain reliable results, it is crucial to implement a complete portion of the catalog. We thus evaluated the minimum magnitude of completeness (M_c) of the catalog based on the maximum curvature approach (Wiemer and Wyss 2000), as shown in Fig. 2a. We modeled the frequency–magnitude distribution of the background seismicity according to the GR law. Based on the analyses, we obtained a *b*-value of 0.78 considering a magnitude threshold of 3.5. Since some previous

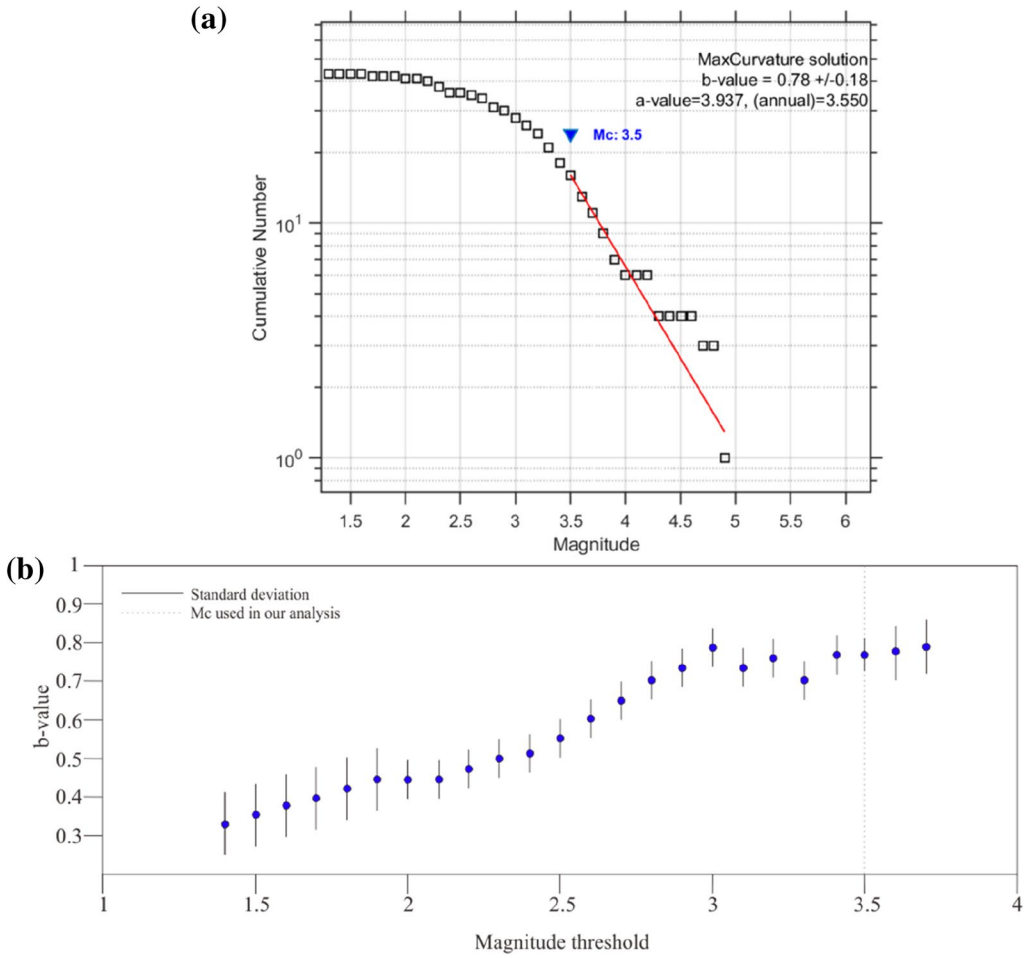

Fig. 2 **a** Magnitude–frequency distribution of the background seismicity in the 3 years before the mainshock and **b** corresponding *b*-values considering different magnitude thresholds. The *b*-value is evaluated based on the events with magnitudes greater than M_c by using the maximum-likelihood technique. The red line represents the best fit of the GR law; open squares represent the cumulative number of observed events as a function of magnitude

studies (e.g., Wiemer and Wyss 2000) concluded that the maximum curvature approach could underestimate M_c, to validate the stability of our analysis, we reported *b*-values considering different magnitude thresholds (Fig. 2b). When the magnitude thresholds are between 2.9 and 3.7, the estimated *b*-values are similar (ca. 0.7–0.8), confirming the stability of the procedure. Based on this procedure, we implemented the seismicity 1 year before the mainshock, including 29 events with $M \geq 3.2$, and determined a significantly low *b*-value of 0.45 (Additional file 1: Figure S1). We have confirmed the difference of the *b*-value is larger than the reported standard deviation.

The above analyses indicate a low b-value anomaly in the temporal distribution leading up to the Pasaman earthquake. It is important to note that the Mw5.2 foreshock (indicated by the blue circle in Fig. 1) caused a decrease in the b-value, with the value dropping from 0.78 (Fig. 2a) to 0.69 when the foreshock is taken into account. This anomalous b-value may be indicative of a potential precursor to the impending mainshock. The *b*-value anomaly could indicate stress accumulation in the area and the future occurrence of an earthquake (Main et al. 1989). In addition, such a decreasing temporal trend could be significant, even considering the uncertainties from the magnitude threshold and uncertainties of *b*-values (Fig. 2b). Based on this concept, monitoring the evolution of *b*-values could illustrate tectonic stress and provide a better understanding of future seismic hazards along the Sumatran Fault system.

Spatial and temporal distribution of aftershocks. Within 18 days after the Pasaman earthquake mainshock, 217 aftershocks occurred, as reported by BMKG (Fig. 1). The lineation of the aftershock distribution (NW striking) can be associated with the Sumatran Fault system. The aftershocks fill the gap between the Angkola and Sianok segments.

Many aftershocks happened immediately after the mainshock, with the occurrence rate decaying over time. To quantify the aftershock rate evolution, we reported the time interval between each two aftershocks and converted it into a daily interval rate (blue circles in Fig. 3b). This showed a significantly higher rate than the background interval rate before this sequence and that the daily interval rate is more than 10 times higher than the background rate even 18 days after the mainshock (the end of the available catalog). When we were determining how to model the temporal evolution of aftershock sequences, we were aware that the space–time epidemic type aftershock sequence (also known as "ETAS"; Ogata 1988) model might well illustrate the distribution of aftershocks in time and space. Considering the complete

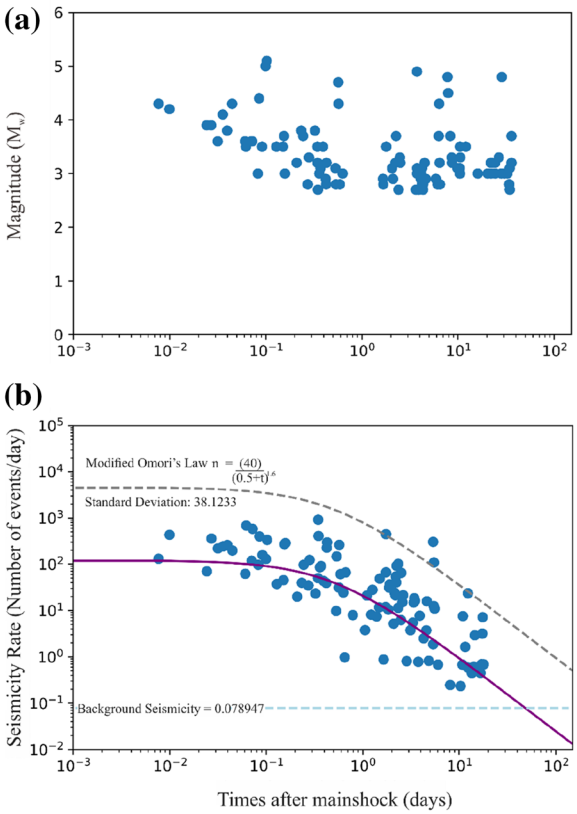

Fig. 3 **a** The magnitudes of the observed aftershocks as a function of time after the mainshock (in days) and **b** the modeled (purple line) and observed (blue circles) temporal distribution of the seismicity rates for the Pasaman earthquake aftershock sequence. The modeled distribution was obtained using the modified Omori's law (Utsu 1961) through regression of the observations. The standard deviation of the regression is shown in dashed grey lines. The background seismicity rate was evaluated according to the seismicity 3 years before the Pasaman earthquake (dashed blue line)

part of the catalog, however, the remaining events are insufficient to propose a reliable ETAS model. Thus, we alternatively modeled the seismicity through the modified Omori's law (Utsu 1961, shown in Eq. 2). Through regression, we obtained the best fits of *K*, *P*, and *C*, which resulted in the rate evolution of the aftershocks being expressed as:

$$n = \frac{40}{(0.5+t)^{1.6}} \pm 38.12. \quad (7)$$

Considering the daily seismicity rate before this sequence (0.079 events per day), this aftershock sequence could last 49 to 473 days, taking into account the average and deviation of the Omori decay, respectively (Fig. 3b).

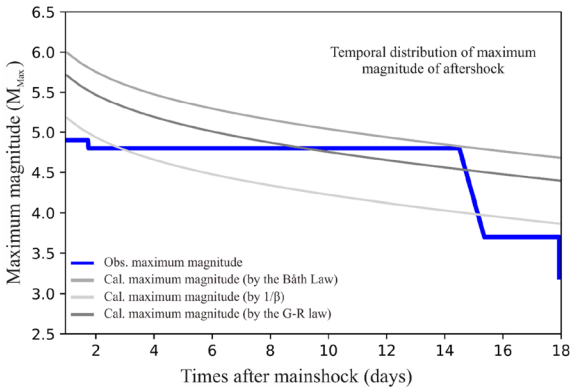

Fig. 4 The observed (blue line) and the modeled (grey lines) temporal distributions of the maximum magnitude of the aftershocks by the Pasaman earthquake using Båth's law, 1/β, and the GR law

We also tried to forecast the maximum magnitude in the aftershock sequence through the following approaches. Considering the relationship of the mainshock (M_w=6.2) and Båth's law (Båth 1965), the maximum largest aftershock (M_1) could be 5.0. With the b-value of 0.88 and 1/β (Utsu 1969), M_1 is 5.7. And based on a- and b-values of 4.63 and 0.88, respectively, we assumed M_1 to be the magnitude with an expected largest event in the aftershock sequence and obtained M_1 of 5.3. The maximum largest aftershock could be further forecast as a function of time (Eq. 3). Based on a t_{end} of 49 days, the temporal evolutions for the maximum magnitude of the aftershocks were forecasted based on various models (Fig. 4). By comparing the modeled temporal distribution of the maximum magnitude with the observation data, our analysis could provide a plausible trend of maximum magnitude in the aftershock sequence.

Coseismic stress evolution associated with subsequent aftershock activity.

An increase in the coseismic Coulomb stress could not only trigger aftershocks, but also enhance the probability of the next larger earthquake. This phenomenon motivated us to comprehensively evaluate the potential seismic hazard from the Sumatran Fault considering the stress change imparted by the Pasaman earthquake.

To estimate the change in the Coulomb stress, an elastic half-space model on an assumed isotropic-homogenous rectangular plane is used (Okada 1992). The ΔCFS calculation in this study is based on the COULOMB 3.3 program (Toda 2005).

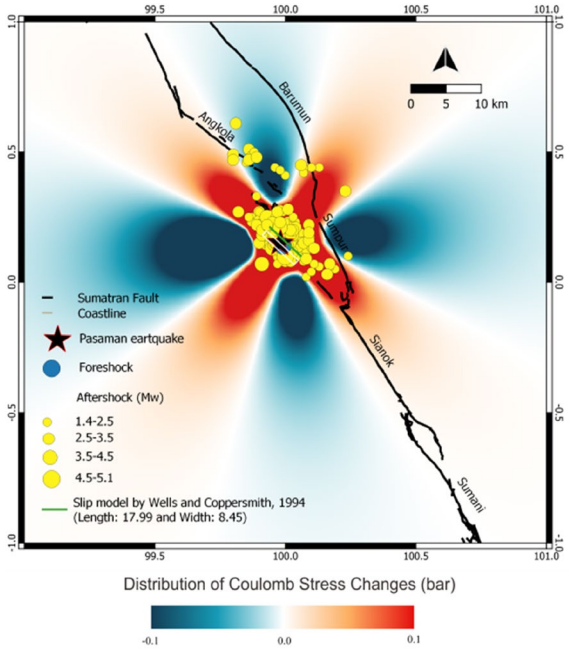

Fig. 5 The Coulomb stress changes imparted by the Pasaman earthquake considering fault rupture geometry models of the scaling law (Wells and Coppersmith 1994) with a length of 17.99 km and width of 8.45 km. The green line is representing the rupture alignment

Our ΔCFS calculation obtained the maximum ΔCFS at different depths among the seismogenic layer since previous studies (e.g., Chan et al. 2012b; Chan 2016) concluded the advantage of this procedure on improving forecasting ability and minimizing calculation uncertainty, especially in the vicinity of the coseismic rupture patch. That is, the uncertainty of slip model geometry along the dip direction could be efficiently eliminated by considering maximum ΔCFS at different depths among the seismogenic layer. According to the study of Collings et al. (2012), the seismogenic depth based on the hypocenter distribution beneath the Sumatra Fault is ca. 20 km. So, we calculated the ΔCFS at depths between 0 and 20 km and reported the maximum one for each calculation grid.

Since the focal mechanisms of the aftershocks are unavailable, we first assumed the receiver plane is consistent with the focal mechanism of the mainshock (Table 1) and will discuss the impact of the receiver planes for ΔCFS calculations. Our assumption is also supported by the focal mechanisms of the previous earthquakes determined by the Global Centroid Moment Tensor. Generally, around the Sumatran Fault there were earthquakes with strike-slip faulting, which can be seen in Fig. 1.

A detailed slip dislocation model for the Pasaman earthquake is yet unavailable for the ΔCFS calculation. Due to the limitation, we proposed several slip dislocation models considering mainshock parameters and spatial distribution of aftershocks. We first followed the procedure proposed by Chan et al. (2012b) to implement a simplified slip dislocation model with a homogeneous slip on a rupture area based on the earthquake parameters and the scaling law of Wells and Coppersmith (1994). The rupture parameters and geometry are presented in Table 1 and Fig. 5, respectively. Note that the geometry of our model is similar as that proposed based on inversion of the teleseismic broadband data by Supendi et al. (2023). Based on this model, ΔCFS is enhanced in the vicinity of the rupture and at the extensions along both sides of the rupture, where most of aftershocks taking place (Fig. 5). Although the hypocentral depth of the mainshock determined by USGS is shallower, inferring a shallow rupture patch, we have confirmed that a rupture at shallow depth obtains a similar ΔCFS pattern as our model (Fig. 5). The similar ΔCFS patterns can be attributed to our calculation procedure that we evaluated the ΔCFS among the seismogenic layer (with depth between 0 and 20 km, Sieh and Natawidjaja 2000) and reported the maximum one for each calculation grid.

We then discussed uncertainty of the ΔCFS calculation by the friction coefficient. We considered different friction coefficients to evaluate the impact on the ΔCFS uncertainty. Considering friction coefficients between 0.2 and 0.8, their patterns are similar (Fig. 6). That is, the ΔCFS increased on the Sumpur and Sianok segments and in the region where most of the aftershocks took place. In the following, we used the conclusion of King et al. (1994) to implement an intermediate value of a friction coefficient of 0.4 for the ΔCFS calculation.

We then evaluated the impact of the receiver plane for the ΔCFS calculation. Some previous studies (e.g., Catalli and Chan 2012; Ishibe et al. 2011, 2015; Toda 2008) indicated that the uncertainty of a ΔCFS calculation could be minimized by considering heterogeneous stress fields or various types of focal mechanisms. In the study region, the evidence from both the geological survey (Sieh and Natawidjaja 2000) and focal mechanisms (Fig. 1) suggests a right-lateral faulting on a vertical rupture plane. We then proposed several ΔCFS models considering different strike orientations based on the focal mechanisms of previous events (Fig. 7). These include the 2007 M_w6.3 (with strike of 149˚), the 2006 M_w5.8 (with strike of 162˚), the 2016 M_w5.0 (with strike of 164˚), the 1977 M_w6.1 (with strike of 312˚), the 1986 M_w5.4 (with strike of 334˚), and the 2009 M_w5.1 (with strike of 355˚). The ΔCFS patterns slightly orientate according to strike orientations, while the general patterns are similar.

Based on the ΔCFS uncertainty tests mentioned above, we have confirmed insignificant differences considering various friction coefficients (Fig. 6) and strike angles for receiver fault planes (Fig. 7) within reasonable ranges. All the cases show the stress increase extended northwest and southeast of the coseismic slip alignment (the green lines in Figs. 5, 6, 7) and forecast the aftershock pattern (yellow circles in Figs. 5, 6, 7).

Seismic hazard from the sumatran fault system

An increase in Coulomb stress could not only trigger aftershocks but also enhance the probability of the next larger earthquake. The Pasaman earthquake took place in the Sumatran Fault system with a potential for devastating earthquakes (Sieh and Natawidjaja 2000). To evaluate the seismic hazard imparted by the Pasaman earthquake, we considered the ΔCFS of the Pasaman earthquake and the fault parameters of the Sumatran Fault. To specify the stress change in these segments, their mechanisms (Table 2) and alignments were implemented in the ΔCFS calculation. A map view of the coseismic ΔCFS illustrates the stress changes imparted by the Pasaman earthquake on each segment of the Sumatran Fault system (Fig. 8). Stress in the Sumpur, Sianok, Sumani, and Angkola segments increased while stress in the Barumun segment dropped. The stress in the Sumpur and Sianok segments was significantly enhanced, with a maximum ΔCFS of 0.1 bar, and the stresses in the Sumani and Angkola segments were slightly enhanced, with a maximum ΔCFS of 0.03 and 0.01 bars, respectively (Table 2). Some of previous studies concluded a stress change of more than 0.01 bar could significantly enhance seismic activity (e.g., Stein 1999; Ma et al. 2005; Chan et al. 2009). The stress increase imparted by the Pasaman earthquake could raise seismic hazard potential in the Sumatran Fault system.

To quantify the impact of the seismicity rate based on ΔCFS, we implemented the rate-and-state friction model (Dieterich 1994, shown in Eq. 6). We followed Chan et al. (2017) and assumed $A\sigma$ to be 0.3 (Chan et al. 2017). We obtained t_{na} from our Omori's model (Fig. 3). Based on the rate-and-state friction model and stress change, the rate perturbation by the Pasaman earthquake could be evaluated at each segment of the Sumatran Fault (Table 2). Due to a significant stress increase in the Sumpur and Sianok segments, we expected a seismicity rate increase of ca. 40%. The seismicity rates in the Sumani and Angkola could rise by 10.5% and 3.4%, respectively;

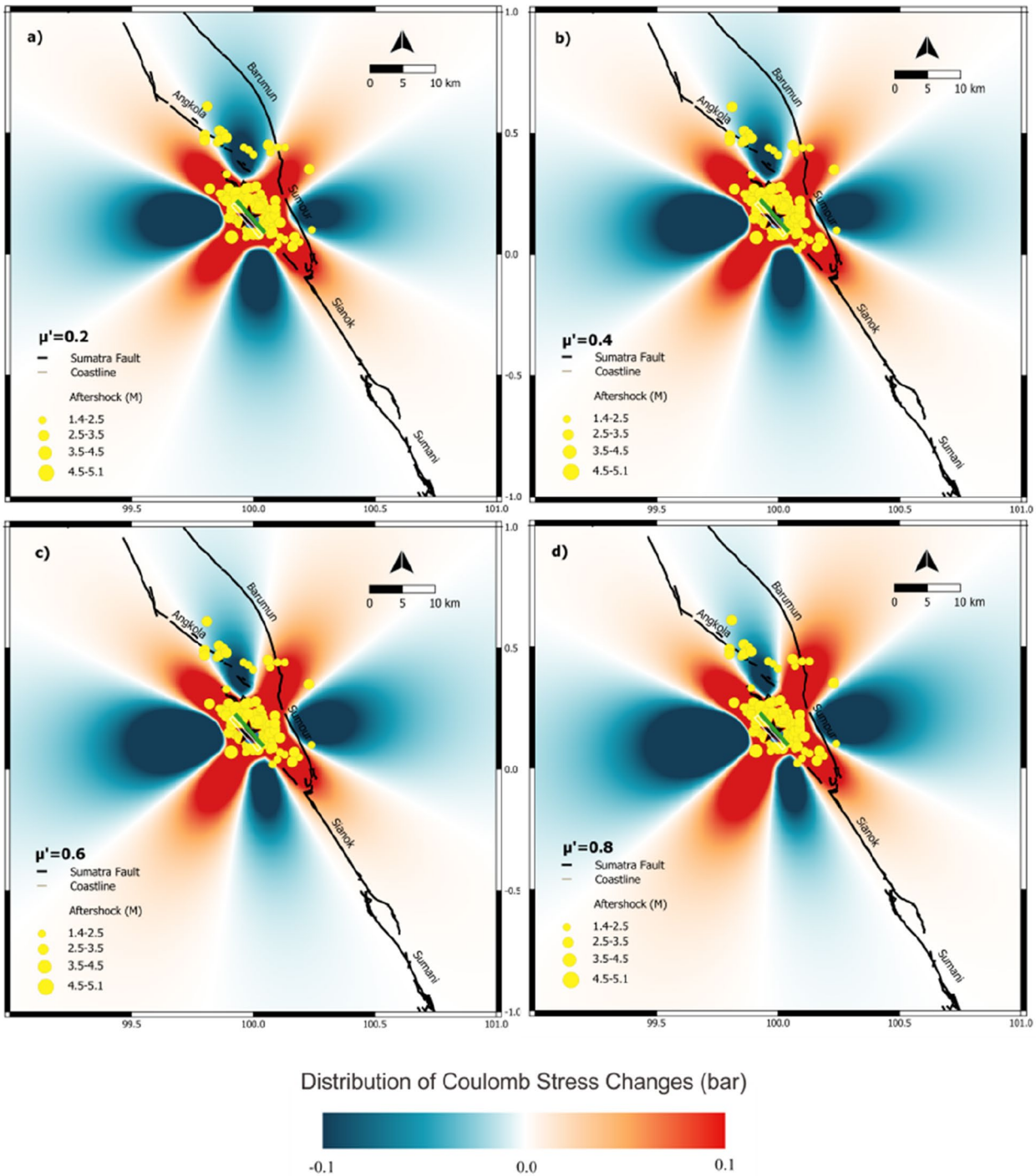

Fig. 6 Stress changes imparted by the Pasaman earthquake considering coefficient frictions of **a** 0.2, **b** 0.4, **c** 0.6, and **d** 0.8. The rupture parameters of the mainshock are shown in Table 1. The specified receiver fault is assumed to be the same as the focal mechanism of the mainshock by BMKG (Table 1). The yellow circles represent aftershocks. The green line is the rupture alignment of the Pasaman earthquake

whereas, the Barumum segment could be farther from the next earthquake due to coseismic stress drop.

The short-term rate perturbation imparted by the Pasaman event has been evaluated for the Sumatran Fault. To quantify its long-term rupture probability, we considered the recurrence interval of each fault segment based on slip rate and maximum magnitudes of the Sumatran Fault reported by Irsyam et al. (2020) in Table 2. The rupture probability could be quantified using a Poisson process, which is widely applied for probabilistic seismic hazard assessment (Cornell 1968), expressed as follows:

$$P = 1 - e^{-\nu \cdot t}, \tag{8}$$

where P represents the rupture probability of a fault, ν represents the annual seismicity rate of the fault segment, and t represents the time period of interest. The Poisson process relies solely on the seismicity rate for a given year, which means that the expected probability should be time independent, regardless occurrence time of last event(s).

Using this model, we quantified each segment's rupture probability in the coming 50 years (Table 2). A high rupture probability of ca. 60% was obtained for the Sumpur segment due to its short recurrence interval (55 years). Generally, the earthquake probabilities on all these segments are rather high due to their high slip rates (14 mm/year).

In addition to the stationary probability based on the assumption of the Poisson process mentioned above, for segments where data from at least one previous earthquake were recorded, evaluation of the rupture probability can be further improved by including the record of the previous earthquake(s). The time elapsed since the previous event could be incorporated into the time-dependent Brownian passage time (BPT) model (Ellsworth et al. 1999). The BPT model has been applied to many probabilistic seismic hazard assessments (e.g., Fujiwara 2014), and its credibility has been confirmed by comparing it to paleo-seismic data (Gao et al. 2022a). The density function (DF) of this model can be represented as:

$$DF = \left(\frac{\mu}{2\pi\alpha^2 t^3}\right)^{1/2} \exp\left(-\frac{(t-\mu)^2}{2\alpha^2 \mu t}\right), \tag{9}$$

where μ represents the mean recurrence interval, t represents the time elapsed since last earthquake, and α represents the aperiodicity, whose value is usually between 0.3 and 0.7 and is assumed to be 0.5 (Chan et al. 2017). Based on this model, the rupture probabilities for the Angkola, Sianok, and Sumani segments (with records of previous events by Sieh and Natawidjaja 2000) were evaluated (shown in Fig. 9). A high rupture probability is expected for a segment with a short recurrence interval and/or long time elapsed since the last earthquake. The earthquake probability at the Sumani segment in the coming 50 years could be 72% (Fig. 9c). Based on the BPT model, these three segments obtained higher rupture probabilities compared to the probabilities obtained via the time-independent Poisson process, which can be attributed to a long time elapsed since the last earthquake.

The BPT model is only applicable for the segments with historical earthquake(s) since application of this model requires the elapsed time since last earthquake (Eq. 9). By contrast, application of the Poisson process only requires annual seismicity rate of the fault segment (Eq. 8) so that we applied this model for all of the segments. In order to validate the performance of the models, Gao et al. (2022b) compared them with paleoseismic data of the Chelungpu fault (Taiwan) and concluded that the BPT model has a better performance. However, it is rather difficult to conduct a similar analysis in the entire Sumatran Fault system due to insufficient historical records.

Due to seismic active with a high slip rate along the Sumatran Fault (Natawidjaja and Triyoso 2007), a high hazard level is expected based on the 2017 national seismic hazard maps of Indonesia (Irsyam et al. 2020). Note that although some segments of the fault have a high slip rate, they do not accumulate a large strain. In this case, these segments could slip through creeping rather than generate a large earthquake. The seismic hazard could be further constrained if the coupling ratios of the fault segments could be further quantified.

Conclusions

This study clarifies the seismicity activity of the Pasaman earthquake sequence and aims to forecast the seismicity in this region and the Sumatran Fault system. Based on the seismicity before the mainshock, a significantly low b-value anomaly was observed. This analysis shed light on the earthquake's precursor via analysis of the evaluation of the b-values prior to the earthquake. We also discussed the spatial and temporal distribution of the aftershocks and modeled them through the coseismic Coulomb stress change imparted by the Pasaman earthquake mainshock and the modified Omori's law, respectively. The outcome could help us understand the pattern of forthcoming aftershocks, including the time duration and the maximum

(See figure on next page.)

Fig. 7 Stress changes imparted by the Pasaman earthquake considering strike angles for receiver planes of **a** 149°, **b** 162°, **c** 164°, **d** 312°, **e** 334, and **f** 355°, corresponding to the focal mechanisms of previous events presented in Fig. 1. The rupture parameters of the mainshock by BMKG are shown in Table 1. The green line is the rupture zone of the Pasaman earthquake. The yellow circles represent the distribution of aftershocks

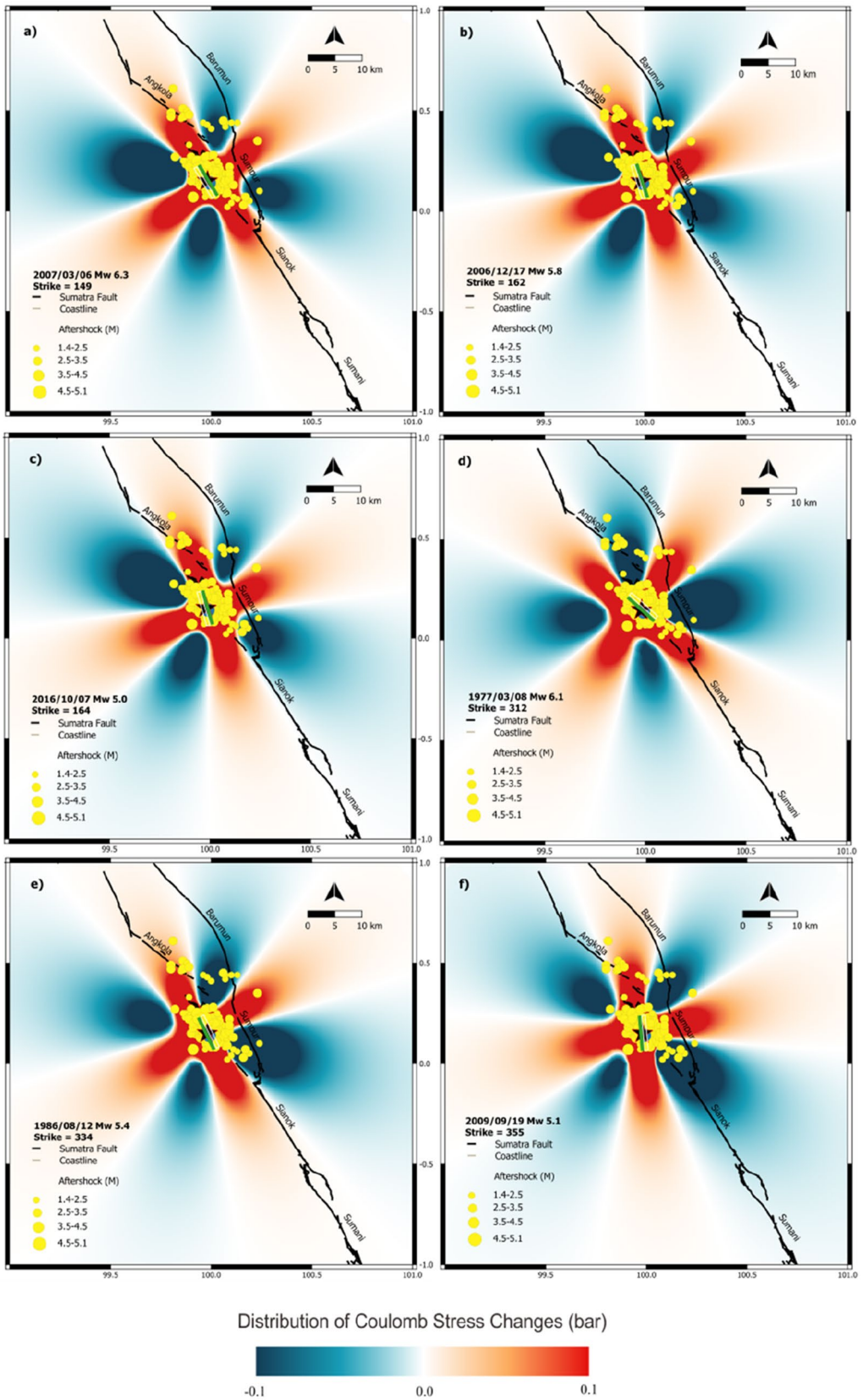

Fig. 7 (See legend on previous page.)

Table 2 The fault parameters for the segment of the Sumatran Fault in the vicinity of the Pasaman earthquake (summarized by Irsyam et al. 2020)

ID	Segment	Last earthquakes	Time elapse (until 2022)	Expected magnitude	Slip rate (mm/yr)	Recurrence interval (year)	Max ΔCFS (bars)	Short-term rate change	Rupture probability in 50 years
1	Angkola	1892	130	7.7	14	291	0.01	3.4%	16.5%
2	Barumun	No record	N/A	7.5	14	192	−0.01	−3.3%	NA
3	Sumpur	No record	N/A	6.9	14	55	0.10	39.6%	NA
4	Sianok	1926	96	7.4	14	156	0.10	39.6%	41.2%
5	Sumani	1943	79	7.1	14	84	0.03	10.5%	72.0%

The records for historical earthquakes were obtained by Sieh and Natawidjaja (2000). The probability of rupture in the next 50 years for each segment is evaluated using the Poisson process and the BPT model for segments where at least one earthquake was recorded

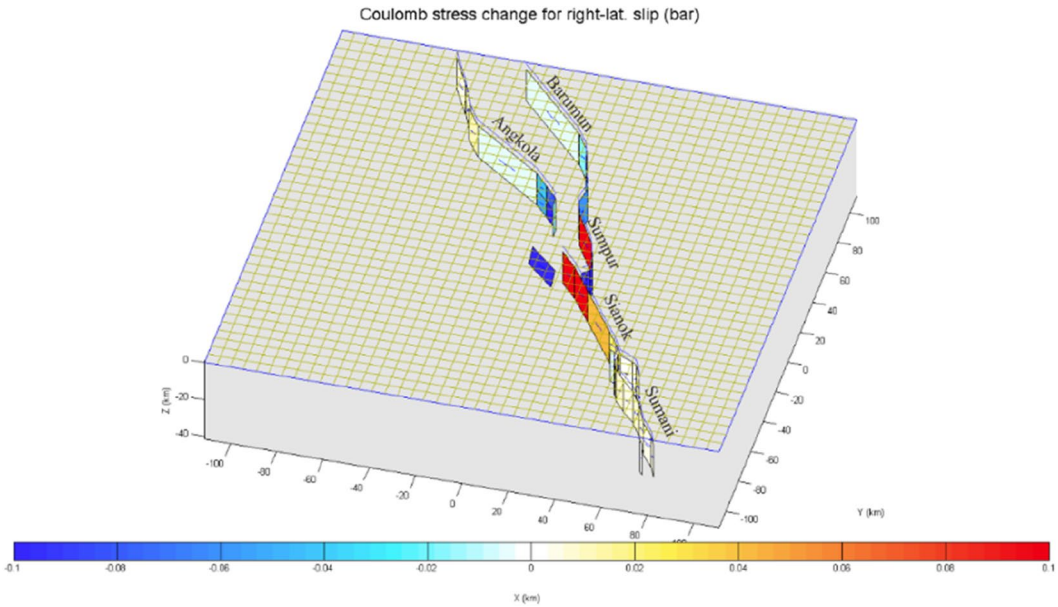

Fig. 8 Coulomb stress changes imparted by the Pasaman earthquake at each segment of the Sumatran Fault. The maximum ΔCFS on each segment is reported in Table 2

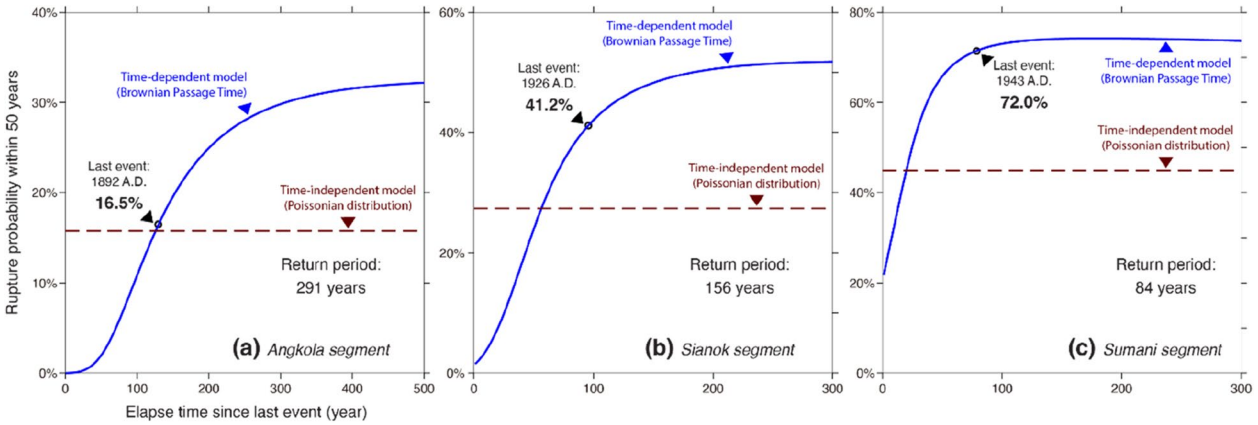

Fig. 9 Rupture probabilities in the coming 50 years for the **a** Angkola, **b** Sianok, and **c** Sumani segments, considering the BPT model (blue solid lines) and Poisson distribution (red dashed lines)

magnitude of aftershock. To evaluate the potential seismic hazard from the Sumatran Fault, fault parameters and coseismic stress of the Pasaman earthquake were implemented to evaluate the rupture probability of each segment. The results suggest the rupture probability of each segment is extremely high. The M_w6.2 Pasaman earthquake rattled Malaysia and Singapore. The next larger events occurring along the Sumatran Fault could result in significantly stronger ground motion and threaten not only Sumatra, but also some metropolises in the far field.

Supplementary Information

The online version contains supplementary material available at https://doi.org/10.1186/s40562-023-00279-6.

Additional file 1: Figure S1. Temporal evolution of **a** Magnitude of completeness (M_c) and **b** *b*-values (solid lines) and standard deviations (dashed lines) for various periods before the Pasaman earthquake. **c** Magnitude-frequency distribution of the background seismicity in each year before the Pasaman earthquake. The earthquakes within 40 km of the Pasaman earthquake were considered for calculation.

Acknowledgements
We thank Shinji Toda and Ross S. Stein for providing Coulomb 3.3. The authors also thank the Agency of Meteorology, Climatology and Geophysics (BMKG) for providing the data, and Kenji Satake, J. Bruce H. Shyu and two anonymous reviewers for their constructive comments.

Author contributions
RW conducted the modeling and performed the analyses, while AW obtained the earthquake catalog. CHC developed the methodologies and administered the project. All authors contributed to scientific discussions, critically validated the results, and participated in writing the manuscript. All authors read and approved the final manuscript.

Funding
This study was supported by the National Science and Technology Council in Taiwan—under grants MOST 109-2116-M-008-029 -MY3, MOST 110-2124-M-002-008, and MOST 110-2634-F-008-008. This work is financially supported by the Earthquake Disaster & Risk Evaluation and Management Center (E-DREaM) from the Featured Areas Research Center Program within the framework of the Higher Education Sprout Project by the Ministry of Education in Taiwan.

Availability of data and materials
The datasets implemented in study are available from the corresponding author upon reasonable request.

Declarations

Ethics approval and consent to participate
Not applicable.

Consent for publication
Not applicable.

Competing interests
The authors declare that they have no known competing financial interests or personal relationships that could have appeared to influence the work reported in this paper.

Author details
[1]Department of Earth Sciences, National Central University, Taoyuan City, Taiwan. [2]Earthquake-Disaster & Risk Evaluation and Management Center, National Central University, Taoyuan City, Taiwan. [3]Indonesian Agency for Meteorology, Climatology, and Geophysics, Jakarta, Indonesia. [4]Geophysical Engineering Study Program, Sumatera Institute of Technology, Lampung, Indonesia.

Received: 18 October 2022 Accepted: 4 May 2023
Published online: 22 May 2023

References

Aki K (1965) Maximum likelihood estimate of b in the formula logN=a-bM and its confidence limits. Bull Earthq Res Inst Tokyo Univ 43(2):237–239
Båth M (1965) Lateral inhomogeneities of the upper mantle. Tectonophysics 2:483–514
Catalli F, Chan CH (2012) New insights into the application of the Coulomb model in real-time. Geophys J Int 188(2):583–599. https://doi.org/10.1111/j.1365-246X.2011.05276.x
Chan CH (2016) Importance of three-dimensional grids and time-dependent factors for applications of earthquake forecasting models to subduction environments. Nat Hazard 16(9):2177–2187
Chan CH, Stein RS (2009) Stress evolution following the 1999 Chi-Chi, Taiwan, earthquake: consequences for afterslip, relaxation, aftershocks and departures from omori decay. Geophys J Int 177(1):179–192. https://doi.org/10.1111/j.1365-246X.2008.04069.x
Chan CH, Wu YM (2013) Maximum magnitudes in aftershock sequences in Taiwan. J Asian Earth Sci 73:409–418. https://doi.org/10.1016/j.jseaes.2013.05.006
Chan CH, Wu YM, Tseng TL, Lin TL, Chen CC (2012a) Spatial and temporal evolution of b-values before large earthquakes in Taiwan. Tectonophysics 532–535:215–222. https://doi.org/10.1016/j.tecto.2012.02.004
Chan CH, Wu YM, Wang JP (2012b) Earthquake forecasting using the rate-and-state friction model and a smoothing Kernel: application to Taiwan. Nat Hazard 12(10):3045–3057
Chan C, Wang Y, Wang Y, Lee Y (2017) Seismic-Hazard assessment over time: modeling earthquakes in Taiwan. Bull Seismol Soc Am 107(5):2342–2352. https://doi.org/10.1785/0120160278
Collings R, Lange D, Rietbrock A, Tilmann F, Natawidjaja D, Suwargadi B, Miller M, Saul J (2012) Structure and seismogenic properties of the Mentawai segment of the sumatra subduction zone revealed by local earthquake traveltime tomography. J Geophys Res: Sol Earth 117(1):1–23. https://doi.org/10.1029/2011JB008469
Cornell BYCA (1968) Owing to the uncertainty in the number, sizes, and locations of future earthquakes it is appropriate that engineers express seismic risk, as design winds or floods are, in terms of return periods (Blume, 1965; Newmark, 1967. Blume, Newmark and c 58(5):1583–1606
Dieterich J (1994) A constitutive law for rate of earthquake production and its application to earthquake clustering. J Geophys Res: Sol Earth 99(2):2601–2618. https://doi.org/10.1029/93JB02581
Ellsworth WL, Matthews MV, Nadeau RM, Nishenko SP, Reasenberg PA, Simpson RW (1999) A physically-based earthquake recurrence model for estimation of long-term earthquake probabilities. US Geol Surv Open-File Rep 99:22
Fujiwara H (2014) Seismic Hazard Maps for Japan. Springer, New York, New york. https://doi.org/10.1007/978-3-642-27737-5_617-1
Gao F, Zielke O, Han Z, Guo P, Gai H, Dai C (2022a) Faulted landforms, slip-rate, and tectonic implications of the eastern Lenglongling fault, northeastern Tibetan Plateau. Tectonophysics 823:229195. https://doi.org/10.1016/j.tecto.2021.229195
Gao JC, Tseng YH, Chan CH (2022b) Validation of the probabilistic seismic hazard assessment by the Taiwan earthquake model through comparison with strong ground motion observations. Seismol Res Lett 93(4):2111–2125
Gardner JK, Knopoff L (1974) Is the sequence of earthquakes in Southern California, with aftershocks removed, poissonian? Bull Seismol Soc Am 64(5):1363–1367
Gutenberg B, Richter CF (1944) Frequency of earthquakes in California*. Bull Seismol Soc Am 34(4):185–188. https://doi.org/10.1785/BSSA0340040185
Harris RA, Simpson RW (1998) Suppression of large earthquakes by stress shadows: a comparison of Coulomb and rate-and-state failure. J Geophys Res: Sol Earth 103(10):24439–24451. https://doi.org/10.1029/98jb00793
Hughes KLH, Masterlark T, Mooney WD (2010) Poroelastic stress-triggering of the 2005 M8.7 Nias earthquake by the 2004 M9.2 sumatra-andaman

earthquake. Earth Planet Sci Lett 293(3–4):289–299. https://doi.org/10.1016/j.epsl.2010.02.043
Irsyam M, Cummins PR, Asrurifak M, Faizal L, Natawidjaja DH, Widiyantoro S, Meilano I, Triyoso W, Rudiyanto A, Hidayati S, Ridwan M, Hanifa NR, Syahbana AJ (2020) Development of the 2017 national seismic hazard maps of Indonesia. Earthq Spectra 36(1_suppl):112–136. https://doi.org/10.1177/8755293020951206
Ishibe T, Shimazaki K, Satake K, Tsuruoka H (2011) Change in seismicity beneath the Tokyo metropolitan area due to the 2011 off the Pacific coast of Tohoku Earthquake. Earth Planets Sp 63:731–735
Ishibe T, Satake K, Sakai S, Shimazaki K, Tsuruoka H, Yokota Y, Nakagawa S, Hirata N (2015) Correlation between coulomb stress imparted by the 2011 Tohoku-Oki earthquake and seismicity rate change in Kanto, Japan. Geophys J Int 201:112–134. https://doi.org/10.1093/gji/ggv001
King GCP, Stein RS, Lin J (1994) Static stress changes and the triggering of earthquakes. Bull-Seismol Soc Am 84(3):935–953. https://doi.org/10.1016/0148-9062(95)94484-2
Ma K-F, Chan C-H, Stein RS (2005) Response of seismicity to coulomb stress triggers and shadows of the 1999 Mw = 76 Chi-Chi, Taiwan, earthquake. J Geophys Res. https://doi.org/10.1029/2004JB003389
Main IG, Meredith PG, Jones C (1989) A reinterpretation of the precursory seismic b-value anomaly from fracture mechanics. Geophys J Int 96(1):131–138. https://doi.org/10.1111/j.1365-246X.1989.tb05255.x
Megawati K, Pan TC, Koketsu K (2003) Response spectral attenuation relationships for Singapore and the Malay Peninsula due to distant sumatran-fault earthquakes. Earthq Eng Struct Dynam 32(14):2241–2265
Natawidjaja DH, Triyoso W (2007) The sumatran fault zone—from source to Hazard. J Earthq Tsunami 01(01):21–47. https://doi.org/10.1142/s1793431107000031
Ogata Y (1988) Statistical models for earthquake occurrences and residual analysis for point processes. J Am Stat Assoc 83(401):9–27
Okada Y (1992) Internal deformation due to shear and tensile faults in a half-space. Bull-Seismol Soc Am 82(2):1018–1040
Schorlemmer D, Wiemer S, Wyss M (2005) Variations in earthquake-size distribution across different stress regimes. Nature 437(7058):539–542. https://doi.org/10.1038/nature04094
Sieh K, Natawidjaja D (2000) Neotectonics of the Sumatran fault, Indonesia. J Geophys Res 105:28295–28326
Stein RS (1999) The role of stress transfer in earthquake occurrence. Nature 402(6762):605–609
Supendi P, Rawlinson N, Prayitno BS, Sianipar D, Simanjuntak A, Widiyantoro S, Palgunadi KH, Kurniawan A, Shiddiqi HA, Nugraha AD, Sahara DP, Daryono D, Triyono R, Adi SP, Karnawati D, Daniarsyad G, Ahadi S, Fatchurochman I, Anugrah SD, Sudrajat A (2023) A previously unidentified fault revealed by the february 25, 2022 (Mw 6 1) Pasaman earthquake West Sumatra, Indonesia. Phys Earth Planet Interi. https://doi.org/10.1016/j.pepi.2022.106973
Toda S (2005) Coulomb 3.3 graphic-rich deformation and stress-change software for earthquake, tectonic, and volcano research and teaching. USGS Open-File Rep 1060:63
Toda S (2008) Coulomb stresses imparted by the 25 March 2007 Mw=6.6 Noto-Hanto, Japan, earthquake explain its 'butterfly' distribution of aftershocks and suggest a heightened seismic hazard. Earth Planets Sp 60:1041–1046
Utsu T (1961) A statistical study on the occurrence of aftershocks. Geophys Mag 30:521–605
Utsu T (1965) A method for determining the value of b in formula log N = a—bM showing the magnitude-frequency relation for earthquakes. Geophys Bull Hokkaido Univ 13:99–103
Utsu T (1969) Aftershock and earthquakes statistics (I). J Fac Sci Hokkaido Univ 3:129–195
Walling M Y, Megawati K, Zhu C. (2012). Estimation of Vs30 Soil Profile Structure of Singapore from Microtremor Records. EGU General Assembly Conference Abstracts
Wang Y, Wang F, Wang M, Shen ZK, Wan Y (2014) Coulomb stress change and evolution induced by the 2008 wenchuan earthquake and its delayed triggering of the 2013 Mw 6.6 lushan earthquake. Seismol Res Lett 85(1):52–59. https://doi.org/10.1785/0220130111
Wells DL, Coppersmith KJ (1994) New empirical relationships among magnitude, rupture length, rupture width, rupture area, and surface displacement. Bull-Seismol Soc Am 84(4):974–1002
Wiemer S (2001) A software package to analyze seismicity: ZMAP. Seismol Res Lett 72(3):373–382. https://doi.org/10.1785/gssrl.72.3.373
Wiemer S, Wyss M (2000) Minimum magnitude of completeness in earthquake catalogs: examples from Alaska, the Western United States, and Japan. Bull Seismol Soc Am 90(4):859–869. https://doi.org/10.1785/0119990114

Publisher's Note